Science Signaling
AAAS

Evolution of CASK into a Mg2+-Sensitive Kinase

Konark Mukherjee, Manu Sharma, Reinhard Jahn, Markus C. Wahl and Thomas C. Südhof (27 April 2010)

Science Signaling **3** (119), ra33. [DOI: 10.1126/scisignal.2000800]

STRUCTURAL BIOLOGY

Evolution of CASK into a Mg^{2+}-Sensitive Kinase

Konark Mukherjee,[1*†] Manu Sharma,[1] Reinhard Jahn,[2] Markus C. Wahl,[3†] Thomas C. Südhof[1†]

(Published 27 April 2010; Volume 3 Issue 119 ra33)

All known protein kinases, except CASK [calcium/calmodulin (CaM)-activated serine-threonine kinase], require magnesium ions (Mg^{2+}) to stimulate the transfer of a phosphate from adenosine 5′-triphosphate (ATP) to a protein substrate. The CaMK (calcium/calmodulin-dependent kinase) domain of CASK shows activity in the absence of Mg^{2+}; indeed, it is inhibited by divalent ions including Mg^{2+}. Here, we converted the Mg^{2+}-inhibited wild-type CASK kinase ($CASK^{WT}$) into a Mg^{2+}-stimulated kinase ($CASK^{4M}$) by substituting four residues within the ATP-binding pocket. Crystal structures of $CASK^{4M}$ with and without bound nucleotide and Mn^{2+}, together with kinetic analyses, demonstrated that Mg^{2+} accelerates catalysis of $CASK^{4M}$ by stabilizing the transition state, enhancing the leaving group properties of adenosine 5′-diphosphate, and indirectly shifting the position of the γ-phosphate of ATP. Phylogenetic analysis revealed that the four residues conferring Mg^{2+}-mediated stimulation were substituted from CASK during early animal evolution, converting a primordial, Mg^{2+}-coordinating form of CASK into a Mg^{2+}-inhibited kinase. This emergence of Mg^{2+} sensitivity (inhibition by Mg^{2+}) conferred regulation of CASK activity by divalent cations, in parallel with the evolution of the animal nervous systems.

INTRODUCTION

Protein kinases constitute ~1.7% of the products of protein-coding genes in the human genome (*1*) and provide valuable targets for therapeutics (*2*). Structural and functional similarities among eukaryotic protein kinases suggest that they evolved from a common ancestor. Thus, protein kinases have an N-terminal lobe, composed of a five-stranded, antiparallel β sheet and a regulatory helix, αC, and a largely α helical C-terminal lobe (*3*). These enzymes use various highly conserved functional motifs for substrate peptide binding, nucleotide binding, and catalysis (*3*). These motifs include an Asp-Phe-Gly (DFG) sequence at the beginning of the activation segment and a conserved asparagine in the catalytic loop of the C-terminal lobe, both of which are involved in Mg^{2+} binding and were believed to be indispensable for kinase-mediated catalysis of phosphate transfer (*3*–*5*). During evolution, some kinases acquired mutations in some of the conserved functional motifs. Noncanonical motifs may satisfy the unique functional requirements of particular kinases, such as an unusual substrate specificity, or they may confer particular catalytic properties (*6*, *7*). Some changes may be detrimental to catalysis, and about 10% of the human protein kinases bearing such changes are classified at present as "pseudokinases" (*8*). Despite their presumed catalytic inactivity, however, many pseudokinases, for example, HER3 (human epidermal growth factor receptor 3) and IRAK2 (interleukin-1 receptor–associated kinase 2), are important signaling molecules.

Many protein kinases bear additional domains that can regulate catalytic activity through autoinhibition, oligomerization, or substrate recruitment (*9*). Thus, although a fundamental level of regulation is implemented through conserved functional motifs within the kinase domain itself, additional domains provide another layer of regulation from outside of the kinase core.

CASK [calcium- and calmodulin-activated serine-threonine kinase] is an essential protein that contains an N-terminal protein kinase domain, followed by elements characteristic of membrane-associated guanylate kinases (MAGUKs), including a PDZ domain, an SH3 domain, and an inactive guanylate kinase domain. CASK, which is highly enriched in brain, binds to cell-adhesion molecules, including neurexins (*10*), syndecans (*11*–*13*), and SynCAM (*14*). Genetic disruption of CASK in mice causes cleft palate, synaptic dysfunction, and lethality (*15*). In humans, mutations in the *CASK* gene are associated with cleft palate, optic atrophy, nystagmus, and mental retardation (*16*–*20*).

The N-terminal kinase domain of CASK most closely resembles those of members of the calcium- and calmodulin-dependent protein kinase (CaMK) subfamily. However, human CASK has a Gly^{162}-Phe^{163}-Gly^{164} (GFG) sequence instead of the Mg^{2+}-binding DFG motif and a cysteine (Cys^{146}) instead of the conserved, Mg^{2+}-binding asparagine in the catalytic loop. Consistent with these substitutions, CASK does not bind Mg^{2+} (*21*). Because Mg^{2+}, which binds adenosine 5′-triphosphate (ATP), was considered an indispensable cofactor for catalytic phosphotransfer, CASK was initially thought to be a pseudokinase (*8*). More recently, however, we found that CASK binds ATP and catalyzes phosphate transfer to the synaptic adhesion molecule neurexin-1, even in the absence of Mg^{2+} (*21*). Indeed, CASK is fully active only in the absence of divalent cations such as Mg^{2+} and Ca^{2+} (*21*). Inhibition of CASK by divalent metal ions would provide an effective mechanism to allow CASK activity in inactive neurons (without divalent cation fluxes) and to shut down the enzyme in active neurons (with divalent cation fluxes) (*21*).

To gain insight into how this atypical Mg^{2+}-sensitive catalytic activity of CASK evolved, we carried out systematic mutagenesis, mechanistic, and structural studies. We found that substitutions of four residues to generate $CASK^{4M}$ turned CASK into a Mg^{2+}-stimulated kinase. Unlike conventional kinases, however, $CASK^{4M}$ retained substantial Mg^{2+}-independent phosphotransfer activity. Structural analysis revealed that, in $CASK^{4M}$, Mg^{2+} accelerates catalysis by stabilizing the transition state, enhancing the leaving group properties of adenosine 5′-diphosphate

[1]Department of Molecular and Cellular Physiology, Stanford University School of Medicine, 1050 Arastradero Road, Palo Alto, CA 94304, USA. [2]Neurobiologie, Max-Planck-Institut für Biophysikalische Chemie, Am Faßberg 11, D-37077 Göttingen, Germany. [3]Fachbereich Biologie, Chemie, Pharmazie, Institut für Chemie und Biochemie, AG Strukturbiochemie, Freie Universität Berlin, Takustrasse 6, D-14195 Berlin, Germany.
*Present address: Biology Department, Brandeis University, MS008, 415 South Street, Waltham, MA 02454-9110, USA.
†To whom correspondence should be addressed. E-mail: konark@brandeis.edu (K.M.); mwahl@chemie.fu-berlin.de (M.C.W.); tcs1@stanford.edu (T.C.S.)

(ADP), and indirectly affecting the position of the γ-phosphate of ATP, suggesting that Mg^{2+} may have similar functions in conventional protein kinases. Although its in vitro activity was strongly stimulated by Mg^{2+} and greater than that of $CASK^{WT}$ (wild-type CASK), $CASK^{4M}$ showed in vivo activity toward neurexin-1 comparable to that of $CASK^{WT}$, suggesting that CASK catalytic activity is optimal for substrates that are recruited through its MAGUK domains. Evolutionary comparison of CASK sequences demonstrated that CASK initially emerged as a conventional Mg^{2+}-stimulated kinase, and later became sensitive to inhibition by Mg^{2+}. The amino acid substitutions that render CASK sensitive to Mg^{2+} occurred early during animal evolution, in parallel with the appearance of the nervous system. Thus, apparently detrimental changes in conserved functional motifs did not lead to the loss of catalytic activity in CASK, but instead may have implemented a novel regulatory mechanism.

RESULTS

Designing a Mg^{2+}-coordinating version of CASK

The CASK CaMK domain is similar in sequence to the corresponding domains of canonical CaMKs, such as CaMKI (≈37% identity) and CaMKII (≈44% identity) (*1*). CaMKI and CaMKII require Mg^{2+} and Ca^{2+} for optimal activity. Mg^{2+} activates phosphotransfer from ATP, whereas Ca^{2+} is required for activation of calmodulin, which counteracts autoinhibition of these enzymes. In contrast, activity of the CASK CaMK domain is inhibited by Mg^{2+} or Ca^{2+} and no metal ion has been found in crystal structures of the CASK CaMK domain in complex with adenine nucleotides (*21*).

Sequence alignments of vertebrate CASKs with human CaMKI and CaMKII revealed substitutions in CASK of residues that are highly conserved in canonical CaMKs; specifically, the Mg^{2+}-binding aspartate of the DFG motif is replaced by a glycine (Gly^{162}), and the Mg^{2+}-binding asparagine of the catalytic loop is replaced by a cysteine (Cys^{146}). In addition to coordinating Mg^{2+}, this asparagine stabilizes the position of an essential aspartate in the catalytic loop (*22*, *23*). We hypothesized that, after the initial merger of a Mg^{2+}-coordinating CaMK domain with the MAGUK domains during evolution, amino acid changes at these two positions led to the loss of Mg^{2+} binding by CASK. To test this hypothesis, we converted Gly^{162} and Cys^{146} of CASK to the canonical Asp and Asn residues, respectively, and assessed binding of the mutants to an ATP analog [TNP-ATP, 2′,3′-*O*-(2,4,6- trinitrophenyl) ATP] in the absence and presence of Mg^{2+}. Neither the single G162D or C146N mutants nor the double mutant enabled CASK binding to TNP-ATP in the presence of Mg^{2+}, although they both bound to TNP-ATP in absence of Mg^{2+} (Fig. 1).

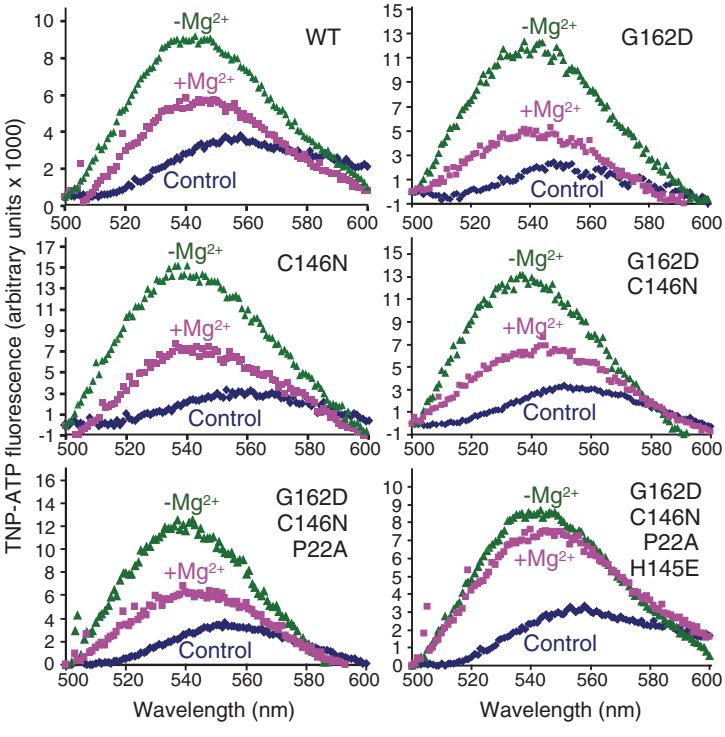

Fig. 1. Designing a Mg^{2+}-coordinating version of CASK CaMK domain. Fluorescence emission spectra of TNP-ATP in the presence of WT and mutant CASK CaMK domains. The protein analyzed (WT or mutant) is indicated in the upper right corner. Dark blue trace: control spectrum of TNP-ATP (1 μM) in tris-HCl buffer (pH 7.0) with EDTA (4 mM). Green trace: spectra of samples containing 1 μM of the indicated recombinant CASK CaMK domain, TNP-ATP (1 μM) and EDTA (4 mM) in tris-HCl buffer (pH 7.0). Magenta trace: spectra of samples containing 1 μM of the indicated recombinant CASK CaMK domain, TNP-ATP (1 μM) and 100 μM $MgCl_2$ in tris-HCl buffer (pH 7.0). Samples were excited at 410 nm, and spectra were recorded between 500 and 600 nm. The spectra are representatives of experiments repeated three times with essentially identical results. Amino acid abbreviations: A, Ala; C, Cys; D, Asp; E, Glu; G, Gly; N, Asn; and P, Pro.

Further sequence analysis revealed two additional deviations from canonical CaMKs in residues that line the CASK nucleotide-binding pocket and could therefore affect Mg^{2+}-ATP binding. Pro^{22} (which corresponds to a conserved alanine in conventional CaMKs) could stiffen the Gly-rich loop (involved in binding ATP), which consequently may lack sufficient flexibility to accommodate the Mg^{2+}-ATP complex. Moreover, Pro^{22} cannot form a hydrogen bond with ATP phosphates because it lacks a backbone NH group. In addition, His^{145} in CASK replaces a negatively charged glutamate immediately preceding the Mg^{2+}-coordinating Asn of the canonical CaMK catalytic loop.

To determine whether these additional changes in conserved residues contribute to the loss of Mg^{2+}-coordination in CASK, we combined mutation of Pro^{22} and His^{145} to the canonical Ala and Glu residues, respectively, with the initial G162D and C146N mutations. A CASK mutant containing G162D, C146N, and P22A still failed to bind TNP-ATP in the presence of Mg^{2+} (Fig. 1). Only the quadruple mutant containing G162D, C146N, P22A, and H145E, which we called $CASK^{4M}$, bound TNP-ATP in the presence of Mg^{2+} (Fig. 1). The increase in fluorescence associated with TNP-ATP interaction with the $CASK^{4M}$ CaMK domain was abolished by excess ATP, indicating that TNP-ATP specifically mimics ATP (fig. S1A).

Comparison of the catalytic properties of $CASK^{WT}$ and $CASK^{4M}$

The ability of ATP to bind $CASK^{4M}$ in the presence of Mg^{2+} suggested that $CASK^{4M}$ may behave catalytically like a conventional, Mg^{2+}-dependent CaMK. To test this notion, we evaluated the kinase activity of CASK mutants in the presence of Mg^{2+}-ATP and excess autocamtide-2 (a synthetic peptide substrate for CaMKII). Consistent with the results with Mg^{2+}-ATP binding, only the quadruple $CASK^{4M}$ mutant consumed ATP in the presence of Mg^{2+} and substrate (Fig. 2A) and showed an increase in autophosphorylation in the presence of Mg^{2+} compared to that in its absence (about a 300% increase under saturating conditions, Fig. 2B; about a 3000% increase under limiting conditions, fig. S2A). All CASK mutants,

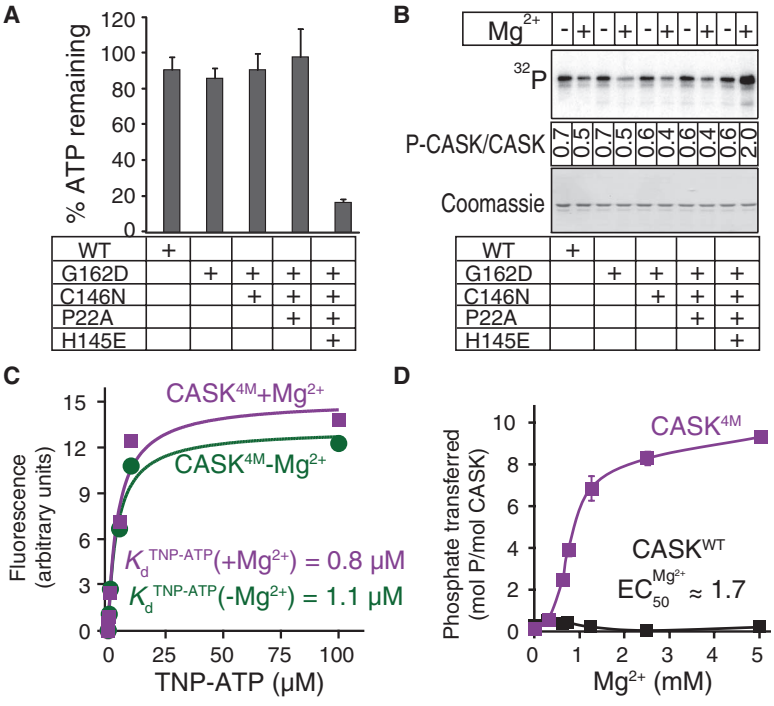

Fig. 2. Effect of divalent ions on nucleotide binding and hydrolysis. (**A**) ATP consumption by WT or mutant CASK CaMK domain. The indicated variants of CASK CaMK domain, autocamtide-2, and Mg^{2+}-ATP were incubated for 60 min as mentioned in Materials and Methods. The remaining ATP was detected with KinaseGlo. The plot represents means ± SD; $n = 3$ experiments. (**B**) Autophosphorylation of WT and mutant CASK CaMK domains. Indicated variants of CASK CaMK domain were incubated with 10 mM Na^+- [γ^{32}P]ATP (–Mg^{2+}) or Mg^{2+}-[γ-^{32}P]ATP (+Mg^{2+}) (50 cpm/mol each) at 30°C with shaking for 2 hours. Upper panel: autoradiogram from phosphorimager scan; lower panel: Ponceau staining. Mean stoichiometry of phosphate incorporation (phosphates per CASK molecule) from three independent experiments is shown. (**C**) TNP-ATP binding. Increasing amounts of TNP-ATP were added to cuvettes containing 1 μM $CASK^{4M}$ and either 4 mM EDTA (magenta) or 200 μM Mg^{2+} (green). Net increase in fluorescence (excitation, 410 nm; emission, 541 nm) is plotted against TNP-ATP concentration. The plot is representative of three independent experiments. (**D**) Effect of Mg^{2+} on $CASK^{4M}$ activity. Indicated variants of CASK CaMK domain, autocamtide-2, and [γ-^{32}P]ATP (250 μM; 250 cpm/pmol) were incubated for 10 min with increasing amounts of Mg^{2+}. The amount of phospho-autocamtide-2 generated was estimated by scintillation counting. Data are presented as means ± SEM ($n = 3$ experiments). EC_{50}, median effective concentration.

including $CASK^{4M}$, bound ATP (Fig. 1) and autophosphorylated themselves (Fig. 2B) in the absence of Mg^{2+}, retaining an activity of CASK that is not present in canonical CaMKs. Thus, $CASK^{4M}$ appears to combine the Mg^{2+}-stimulated activity of classical CaMKs and the Mg^{2+}-independent activity of $CASK^{WT}$. It therefore represents a valuable tool to investigate the catalytic roles of divalent metal ions in kinase reactions.

Mg^{2+}-dependent enhancement of $CASK^{4M}$ catalytic efficiency

Various functions have been suggested for Mg^{2+} in kinase catalysis, including facilitation of nucleotide binding, effects on association or dissociation (or both) of the substrate peptide, and stabilization of the phosphotransfer transition state (*22*, *24*–*26*). To clarify the contribution of Mg^{2+} to phosphotransfer catalysis, we first determined whether the Mg^{2+}-coordinating ability of $CASK^{4M}$ altered its ATP binding (assessed by its interaction with TNP-ATP).

TNP-ATP binding to $CASK^{4M}$ was similar with or without Mg^{2+} (Fig. 2C) and resembled that of $CASK^{WT}$ without Mg^{2+} (fig. S3A). However, ATP competed with TNP-ATP for binding to $CASK^{4M}$ slightly better in the presence of Mg^{2+} than in its absence, indicating that Mg^{2+} might increase the affinity of ATP for $CASK^{4M}$ (fig. S3B). The effect of Mg^{2+} on ATP affinity is masked in direct TNP-ATP affinity measurements, suggesting that it is comparatively small, perhaps because of additional Mg^{2+}-independent contacts of TNP-ATP with $CASK^{4M}$. We also examined the enzymatic parameters of $CASK^{4M}$-mediated phosphotransfer in the absence and presence of Mg^{2+}. Efficient autophosphorylation was observed in the presence of Mg^{2+} (fig. S4). Moreover, catalysis, as determined by $CASK^{4M}$-mediated transfer of phosphate onto autocamtide-2, was robustly enhanced by Mg^{2+} (Fig. 2D). It is unlikely that the strong enhancement of catalytic efficiency of $CASK^{4M}$ by Mg^{2+} results from the mild effect of Mg^{2+} on nucleotide affinity that we observed (see above). Therefore, our results suggest additional roles for Mg^{2+} downstream of ATP binding.

Overall structural comparison of $CASK^{WT}$, $CASK^{4M}$, and CaMKII

To identify the sources of the mechanistic differences between $CASK^{WT}$, $CASK^{4M}$, and CaMKII, we conducted crystal structure analyses. We crystallized the CaMK domain of $CASK^{4M}$ under conditions similar to those we previously used for the CaMK domain of $CASK^{WT}$ and solved the structure by molecular replacement at 2.0 Å resolution (Table 1). The $CASK^{4M}$ CaMK domain exhibits a typical protein kinase fold, with an N-terminal lobe dominated by a five-stranded β sheet and a primarily α helical C-terminal lobe (Fig. 3A). The C-terminal lobe is followed by a loop (residues 286 to 288) and an α helix, αR1 (residues 289 to 303; Fig. 3, A and B), which are not part of the canonical kinase core. The overall structure of the $CASK^{4M}$ CaMK domain is substantially closer to that of $CASK^{WT}$ [Protein Data Bank (PDB) IDs 3C0G and 3C0I; root mean square deviation (RMSD) 0.43 to 0.61 Å for 302 matching Cα atoms; (*21*)] than to that of CaMKII crystallized in an autoinhibited conformation [PDB ID 2BDW; RMSD 1.47 to 1.95 Å for 260 to 276 matching Cα atoms (*27*)] (Fig. 3, A to C). Therefore, the four amino acid substitutions that confer Mg^{2+}-stimulated kinase activity on $CASK^{4M}$ do not alter the overall structure of its CaMK domain.

β- and γ-phosphate positioning of bound AMPPNP is altered by divalent ion

To investigate the presumed additional role of Mg^{2+} beyond its facilitation of nucleotide binding, we determined the crystal structures of $CASK^{4M}$ in complex with either Na^+-adenylyl-imidodiphosphate (AMPPNP) or Mn^{2+}-AMPPNP (Table 1). AMPPNP is a nonhydrolyzable analog of ATP, and Mn^{2+} is considered a stereochemical equivalent of Mg^{2+} (*22*, *23*). Consistent with the TNP-ATP binding data (Figs. 1 and 2C), $CASK^{4M}$ coordinated AMPPNP even in the absence of divalent metal ions (Fig. 4A). Conversely, after soaking $CASK^{4M}$ crystals with Mn^{2+} solution, we failed to discern a bound divalent ion in the absence of AMPPNP (fig. S5A), suggesting that Mg^{2+} is coordinated only when complexed with a nucleotide.

Table 1. Crystallographic data and refinement. ESU, estimated overall coordinate error based on maximum likelihood.

	Native	AMPPNP	Mn^{2+}	AMPPNP-Mn^{2+}
		Data collection		
Wavelength (Å)	0.91841	0.91841	1.87856	1.87856
Temperature (K)	100	100	100	100
Space group	$P2_12_12_1$	$P2_12_12_1$	$P2_12_12_1$	$P2_12_12_1$
Unit cell (Å)				
a, *b*, *c*	58.7, 61.8, 100.2	59.0, 62.2, 97.9	58.9, 61.8, 101.5	58.9, 62.0, 100.6
Resolution (Å)	30.0–2.0 (2.06–2.00)*	50.0–2.1 (2.16–2.10)	50.0–2.2 (2.24–2.20)	20.0–2.3 (2.36–2.30)
Reflections				
Unique	25713 (1829)	21482 (1899)	35224 (1513)†	31058 (1968)†
Completeness (%)	98.4 (94.5)	97.7 (97.1)	96.9 (84.4)	98.2 (83.8)
Redundancy	6.7 (6.2)	5.2 (4.9)	4.7 (2.7)	4.5 (2.7)
$I/\sigma(I)$	29.0 (3.3)	15.9 (2.4)	11.3 (1.3)	14.4 (2.2)
$R_{sym}(I)$‡	3.6 (49.2)	5.7 (58.9)	9.0 (56.8)	6.3 (49.7)
		Refinement		
Resolution (Å)	30.0–2.00 (2.05–2.00)	30.0–2.10 (2.15–2.10)	30.0–2.20 (2.26–2.20)	20.0–2.30 (2.36–2.30)
Reflections				
Number	24,959 (1727)	21,153 (1516)	18,858 (1180)	16,714 (1046)
Completeness (%)	98.6 (94.3)	97.7 (96.6)	97.0 (84.2)	100.0 (100.0)
Test set (%)	5.1	5.1	5.1	5.0
R_{work}§	19.6 (24.8)	21.9 (29.7)	21.0 (28.5)	17.9 (20.9)
R_{free}§	24.1 (31.5)	26.8 (29.6)	27.0 (39.9)	23.4 (30.9)
ESU (Å)	0.14	0.20	0.19	0.17
Refined atoms				
Protein	2461	2446	2422	2430
Water	235	199	141	196
Ligands	19	31	–	32
Mean *B* factors (Å^2)				
Wilson	30.4	33.7	35.1	51.1
Protein	38.0	46.1	35.6	43.1
Water	46.2	46.3	38.5	46.9
Ligand	65.5	63.5	–	54.2
Ramachandran plot (%)¶				
Favored	96.0	94.4	97.0	95.7
Outliers	1.0	1.0	0.7	1.0
RMSD target geometry				
Bond lengths (Å)	0.011	0.011	0.010	0.010
Bond angles (°)	1.322	1.209	1.248	1.324
RMSD *B* factors (Å^2)				
Main-chain bonds	0.661	0.437	0.549	0.589
Main-chain angles	1.064	0.741	0.942	1.033
Side-chain bonds	1.554	1.099	1.316	1.523
Side-chain angles	2.277	1.719	2.110	2.493
PDB ID	3MFR	3MFS	3MFT	3MFU

*Data for the highest-resolution shell in parentheses. †Mn^{2+} and AMPPNP-Mn^{2+} data sets were processed without merging Friedel pairs. ‡$R_{sym}(I) = \sum_{hkl}\sum_i |I_i(hkl) - \langle I(hkl)\rangle| / \sum_{hkl}\sum_i |I_i(hkl)|$, for *n* independent reflections and *i* observations of a given reflection; $\langle I(hkl)\rangle$ is the average intensity of the *i* observations. §$R = \sum_{hkl}||F_o| - |F_c|| / \sum_{hkl}|F_o|$; R_{work} – $hkl \notin T$; R_{free} – $hkl \in T$; *T*-test set. ¶Calculated with MolProbity (http://molprobity.biochem.duke.edu/).

The overall orientation of the AMPPNP adenosine moiety was similar in the presence or absence of Mn^{2+} (Fig. 4, A and B), and AMPPNP could be modeled in a similar orientation into the nucleotide-binding pocket of $CASK^{WT}$ without steric clashes, suggesting that the global positioning of ATP and the orientation of the base moiety is not affected by the divalent cation. However, the orientation of the β- and γ-phosphates of AMPPNP was specifically altered by Mn^{2+} in $CASK^{4M}$ (Fig. 4, A and B). We therefore conclude that the primary role of Mg^{2+} in the nucleotide-binding pocket of $CASK^{4M}$ is coordinating and positioning of β- and γ-phosphates of ATP independent of the positioning of the adenosine moiety, a conclusion consistent with previous studies on the effects of Mg^{2+} on nucleotide interactions with protein kinase A (PKA) (*28*, *29*).

Role of Mg^{2+} in kinase catalysis

The manner in which Mg^{2+} ions bind ATP phosphates in kinase active sites varies with different kinases (*22*, *30*). To unequivocally locate divalent metal ions in the Mn^{2+}-AMPPNP complex at the $CASK^{4M}$ CaMK domain, we measured diffraction at an x-ray wavelength of 1.88 Å, where Mn^{2+} exhibits a measurable anomalous signal, and calculated anomalous difference Fourier maps. This revealed a single coordinated Mn^{2+} ion in the co-crystal structure of Mn^{2+}-AMPPNP with the $CASK^{4M}$ CaMK domain (Fig. 4C).

Similar to its role in some conventional kinases, such as death-associated protein kinase 1 (DAPKI) and mitogen-activated or extracellular signal-regulated protein kinase kinase 1 (MEK1) (*31*, *32*), the Mn^{2+} ion in the $CASK^{4M}$ CaMK domain coordinates the β-phosphate of AMPPNP and

therefore can only indirectly affect orientation of the γ-phosphate (Fig. 4C). Therefore, we surmise that the role of Mg^{2+} in enhancing kinase catalysis is to enhance the leaving group properties of ADP by compensating for additional negative charge that evolves at the β-phosphate during the reaction, by stabilizing the transition state, as well as by indirectly altering the position of the γ-phosphate. Together, our observations are consistent with the notion at Mg^{2+} coordinates the ATP phosphates to favor a catalytically productive kinase-ATP complex (*22–24*, *33*, *34*).

Identification of His^{145} as a possible $CASK^{WT}$ Mg^{2+} sensor

The conformations of the residues lining the ATP-binding pockets of the $CASK^{4M}$ (this work) and $CASK^{WT}$ (*21*) kinase domains are similar, with conformational differences strictly limited to the four exchanged amino acids. Ala^{22} and Asn^{146} in $CASK^{4M}$ adopt conformations similar to those of the corresponding Pro^{22} and Cys^{146} in $CASK^{WT}$. Aside from the introduction of the Asp^{162} side chain (instead of Gly^{162} in $CASK^{WT}$), the most pronounced difference is a change in the side-chain orientation of Glu^{145} in $CASK^{4M}$ compared to that of His^{145} in $CASK^{WT}$ [Fig. 4, compare (A) with (D)]. In $CASK^{WT}$, His^{145} protrudes into the nucleotide-binding pocket (Fig. 4D) and spatially overlaps with the region in which a water molecule in the coordination sphere of the Mn^{2+} ion bound in the $CASK^{4M}$-Mn^{2+}-AMPPNP co-crystal structure is found (Fig. 4, B and C). In $CASK^{4M}$, Glu^{145} is sequestered by Arg^{302} from the C-terminal extension and is thereby directed away from the ATP pocket (Fig. 4, A and B, and fig. S5, A and B). A similar situation is seen in CaMKII, where Glu^{139} is pulled away by Arg^{297} (*27*). The G162D-C146N-P22A triple mutant of CASK is inhibited by Mg^{2+} (Fig. 2B), suggesting that His^{145} is not tolerated in the coordination sphere of the divalent metal ion. TNP-ATP binding to $CASK^{WT}$ is partially inhibited by Mg^{2+} at pH 8.8, at which most His side chains are expected to be neutral (fig. S1B). However, local pH is difficult to estimate and His^{145} may remain protonated within the $CASK^{WT}$ ATP-binding pocket. Thus, our data suggest that His^{145} prevents metal coordination in $CASK^{WT}$ by invading the coordination sphere of the incoming metal ion.

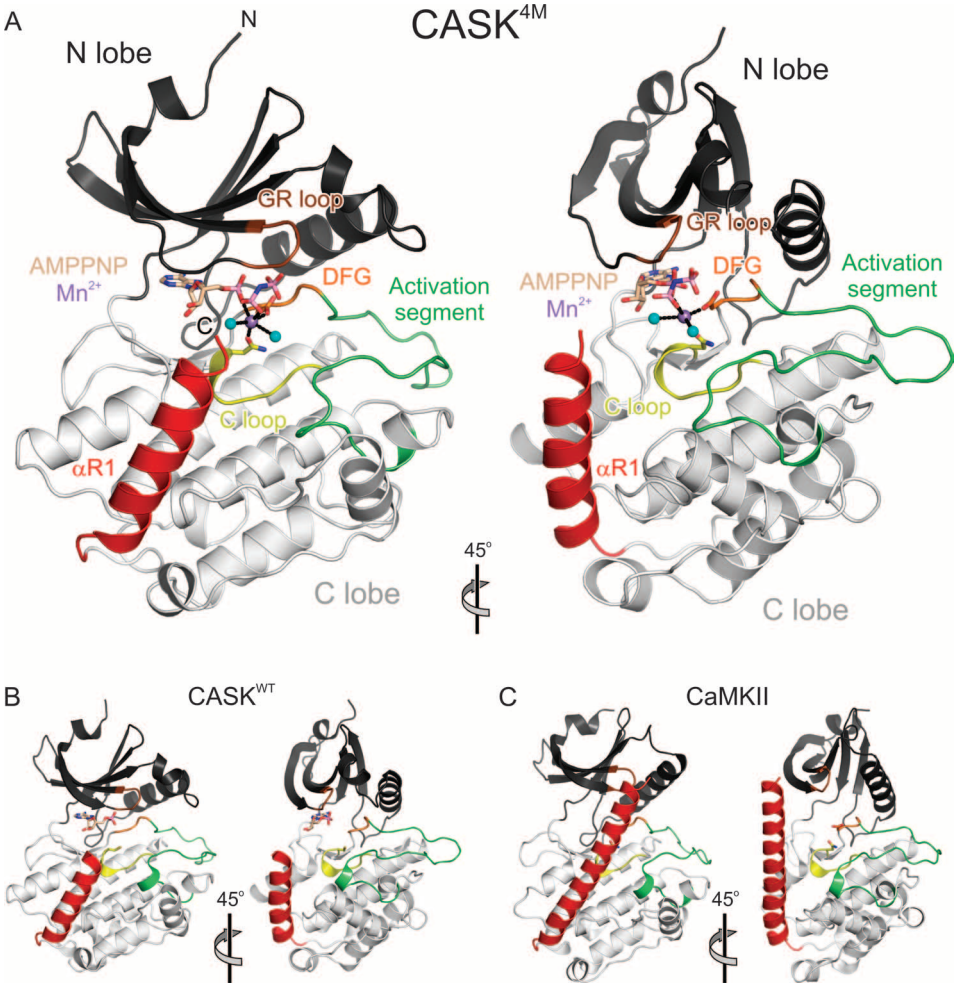

Fig. 3. Overview of the $CASK^{4M}$-Mn^{2+}-AMPPNP crystal structure. (**A**) Orthogonal ribbon plot of $CASK^{4M}$ CaMK domain with landmark functional elements colored. Gly-rich loop (GR loop), brown; catalytic loop (C loop), yellow; DFG motif of the Mg^{2+}-binding loop, orange; activation segment, green; C-terminal Ca^{2+}-CaM-binding element, red. AMPPNP and residues Asn^{146} and Asp^{162}, which coordinate the Mn^{2+} ion, are shown as sticks and colored by atom type. Carbon, beige; oxygen, red; nitrogen, blue; phosphorus, pink. (**B**) Structure of CASK CaMK domain in complex with AMPPNP (sticks) lacking a divalent metal ion [β- and γ-phosphates disordered; PDB ID 3C0H (*21*)] in the same orientation as the $CASK^{4M}$ CaMK domain in (A). Cys^{146} is shown as sticks. Functional elements are colored as in (A). (**C**) Structure of CaMKII kinase domain [PDB ID 2BDW (*27*)] in the same orientation as the $CASK^{4M}$ CaMK kinase domain in (A). Asn^{140} and Asp^{156}, whose equivalents in $CASK^{4M}$ coordinate the Mn^{2+} ion, are shown as sticks. Functional elements are colored as in (A).

Additional features enabling Mg^{2+}-independent activities of $CASK^{WT}$ and $CASK^{4M}$

Although the activity of the $CASK^{4M}$ CaMK domain is strongly stimulated by Mg^{2+}, the enzyme still has catalytic activity in the absence of Mg^{2+} (Fig. 2B). Similarly, $CASK^{WT}$ binds ATP and transfers phosphates to substrate in the absence of Mg^{2+} (*21*). Therefore, CASK must have undergone evolutionary adaptations that are retained in $CASK^{4M}$ and which allow catalysis without Mg^{2+}. For instance, CASK may have acquired features that promote formation of the kinase-ATP-substrate ternary complex and increase substrate phosphorylation under chemically suboptimal conditions (such as in the absence of Mg^{2+}).

Both the $CASK^{WT}$ (*21*) and $CASK^{4M}$ CaMK domains retained bound nucleotide during purification and crystallization in the absence of added nucleotides (Fig. 4D and fig. S5B), unlike other constitutively active kinases such as casein kinase II and PIM1, which are purified in their apo forms (*35*, *36*). We modeled this nucleotide as an adenosine 3′-phosphate molecule (3′-AMP), likely a product of bacterial RNA degradation during cell rupture. The binding mode of 3′-AMP differs from that of AMPPNP binding in either enzyme (compare Fig. 4, A

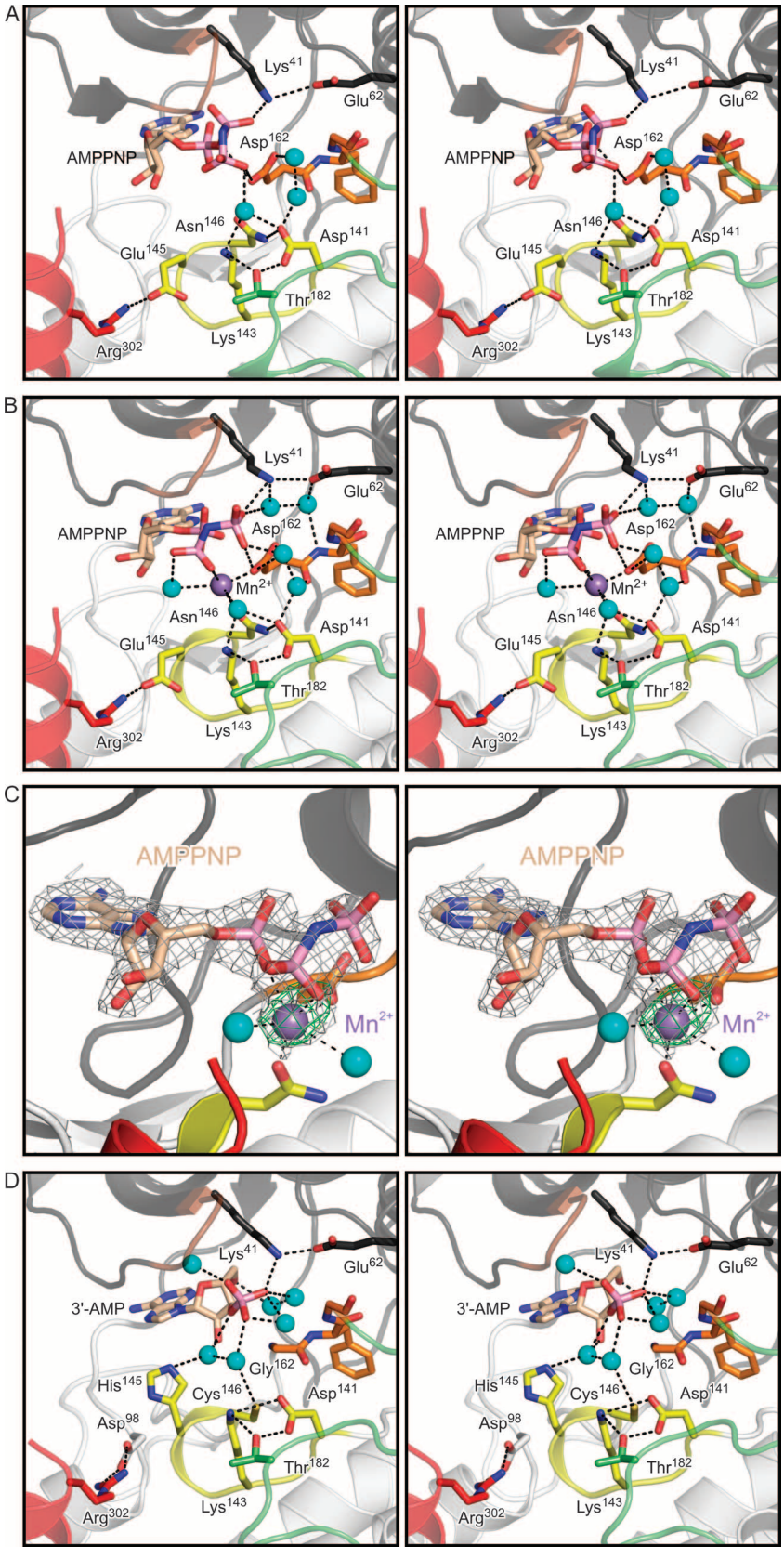

Fig. 4. Nucleotide-binding pocket of the CASK^{4M} CaMK domain. (**A**) Stereo image of CASK^{4M} CaMK domain in complex with AMPPNP without a divalent metal ion. (**B**) Stereo image of CASK^{4M} CaMK domain in complex with AMPPNP-Mn^{2+}. Residues of the Mg^{2+}-binding loop are shown in orange, residues of the catalytic loop are in yellow, and residues of the C-terminal Ca^{2+}/CaM-binding element are in red (as in Fig. 3). Selected residues and the nucleotides are shown as sticks and colored by atom type; carbon, as the respective fragment; oxygen, red; nitrogen, blue; phosphorus, pink. Water molecules (cyan) and the Mn^{2+} ion (purple) are shown as spheres. Orientations are as in Fig. 3A (right panel). The orientations of the AMPPNP β- and γ-phosphates differ in the complexes without and with Mn^{2+} [compare (A) and (B)]. (**C**) Stereo plot showing the final $2F_o - F_c$ electron density around the AMPPNP-Mn^{2+} complex contoured at the 1σ level (gray mesh) and the anomalous difference Fourier map contoured at the 5σ level (green mesh), indicating the position of the Mn^{2+} ion. AMPPNP is shown as sticks and colored by atom type as before. The Mn^{2+} ion (purple) and two coordinating water molecules (cyan) are shown as spheres. Orientation as in Fig. 3A (left panel). (**D**) Stereo image of CASK^{WT} CaMK domain in complex with co-purified 3′-AMP (*21*). Color coding as above. Orientations as in Fig. 3B (right panel).

and B, with Fig. 4D and fig. S5B), and no residual electron density was discerned in the nucleotide-binding pocket of CASK^{4M} after the crystals were washed in Mn^{2+}-containing buffer, indicating that 3′-AMP is easily detached from the pocket (see above and fig. S5A). Nevertheless, co-purification of the nucleotide attests to the general accessibility of the nucleotide-binding pockets of CASK^{WT} and CASK^{4M}. These observations indirectly support the idea that CASK^{WT} and CASK^{4M} adopt a nucleotide-receptive conformation that ensures the unregulated occupancy of their nucleotide-binding pockets by ATP even in the absence of Mg^{2+}.

Features permitting the Ca^{2+}-independent activities of CASK^{WT} and CASK^{4M}

In their active states, protein kinases adopt a conserved conformation of the two lobes, in which their functional elements are poised for substrate binding and catalysis (*3*, *37*). By default, archetypical CaMKs adopt an autoinhibited conformation (*27*, *38*). CaMK activation requires binding of Ca^{2+}-CaM to the autoregulatory domain, leading to its detachment from the catalytic domain and restoration of the active conformation. Therefore, Ca^{2+} is required for optimal catalysis by CaMKs (*27*, *38*).

Immediately after the kinase domain, CASK contains a sequence that is homologous to the autoregulatory domain of CaMKII (residues 281 to 310) and binds to Ca^{2+}-CaM (*10*). Similar to CaMKI and CaMKII, residues 289 to 302 of CASK form a helical extension (αR1) that packs against the C-terminal lobe (Fig. 3 and fig. S6). However, in neither CASK^{WT} (*21*) nor CASK^{4M} does helix αR1 or its C-terminal extension engage in direct contacts with residues of the ATP-binding cleft (Fig. 3A) (*38*). Furthermore, CASK has an arginine-to-leucine substitution in the RXXT/S (R, Arg; X, any amino acid; T, Thr; S, Ser) motif of its autoregulatory domain. A similar mutation in the CaMKII autoinhibitory segment can reduce the affinity of the autoinhibitory segment to the substrate-binding site by more than two log orders (*39*, *40*). Consequently, the CASK^{WT} and CASK^{4M} CaM domains, including the putative autoinhibitory regions, remain compatible with constitutive substrate binding. This allows increased formation of the ternary kinase-ATP-substrate complexes, which may partly compensate for the failure of CASK^{WT} to use the cofactor Mg^{2+}.

Because CASK^{4M} is not inhibited by divalent ions, we were able to directly test the effect of Ca^{2+}-CaM on the rate of catalysis. We first measured the Mg^{2+}-stimulated kinetics of CASK^{4M}-mediated phosphorylation of the CaMKII substrate autocamtide-2 in the absence of Ca^{2+}-CaM. Under these conditions, CASK^{4M} had a V_{max} of ≈1 μmol μmol^{-1} min^{-1} and a Michaelis constant for ATP of ≈70 μM (Fig. 5A). These kinetic parameters are comparable with those of Ca^{2+}-CaM–activated CaMKIV for synapsin I (also a CAMKII substrate) (*41*). Furthermore, Ca^{2+}-CaM had no stimulatory effect on CASK^{4M} catalytic activity (Fig. 5B). Together, the structural and the enzymological data suggest that CASK has a nonfunctional autoinhibitory domain, possibly as an evolutionary vestige of its CaMK ancestors. Consistent with this, both CASK^{WT} and CASK^{4M}, unlike CaMKII, show autophosphorylation in the absence of divalent ions (fig. S2C). Whether Ca^{2+}-CaM binding to CASK has another physiological role remains to be determined.

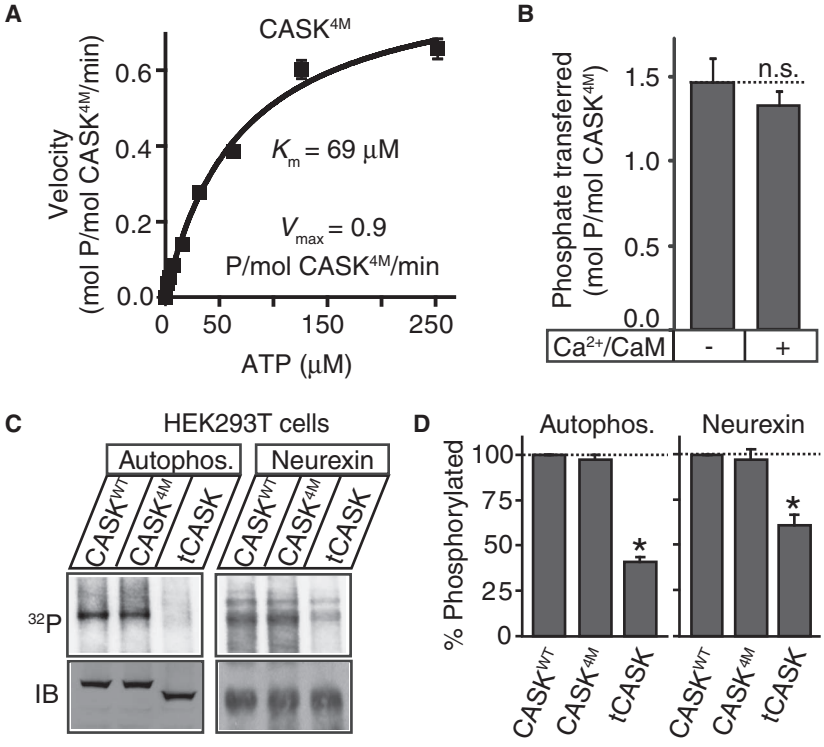

Fig. 5. Compensation for slow kinetics in CASK kinase activity. (**A**) Catalytic kinetics of CASK^{4M}. Purified CASK^{4M} CaMK domain (2 μM) was incubated with increasing amounts of [γ-^{32}P]ATP (400 cpm/pmol) in tris-HCl buffer (pH 7.0) containing Mg^{2+} (10 mM) and autocamtide (100 μM) as the substrate peptide for 10 min at 30°C. Amount of ^{32}P incorporated in autocamtide-2 was measured. Data shown are means ± SEM (n = 3 experiments). (**B**) Effect of Ca^{2+}/CaM on the catalytic rate. CASK^{4M} CaMK domain (2 μM) was incubated with [γ-^{32}P]ATP (200 μM, 800 cpm/pmol) in tris-HCl buffer (pH 7.0) supplemented with Mg^{2+} (2 mM) and autocamtide-2 (100 μM) for 2 min in the presence or absence of Ca^{2+} (1 mM) and CaM (10 μM). The amount of ^{32}P incorporated in autocamtide-2 was measured. Data are presented as means ± SEM, n = 3 experiments. n.s., not significant. (**C** and **D**) Neurexin phosphorylation. Phosphorylation was performed in HEK293T cells transfected with Flag epitope–tagged neurexin and EGFP-CASK, EGFP-CASK^{4M}, or truncated EGFP-tCASK. Autophosphorylation of the coprecipitated CASK (Autophos.) and phosphorylated neurexin (Neurexin) are shown. Immunoblotting (IB) for neurexin and CASK was performed to show expression. The bar graph depicts the comparison of autophosphorylation or neurexin phosphorylation levels in cells coexpressing the indicated CASK variants. Data are presented as means ± SEM, n = 3 experiments; *P < 0.05.

Similar intracellular kinase activities of CASK^{WT} and CASK^{4M}

CASK^{4M} catalytic activity was stimulated by Mg^{2+} and its in vitro activity was considerably higher than that of CASK^{WT} activity either in the presence or absence of Mg^{2+} (Fig. 2, B and D, and fig. S2, A and B). In cells, most of ATP is bound to Mg^{2+}. We therefore wondered whether full-length CASK^{4M} would elicit higher target phosphorylation compared to full-length CASK^{WT} in a cytosolic milieu. Neurexin-1 is at present the only characterized in vivo substrate of CASK (*21*). Neurexin-1 was cotransfected with full-length CASK^{WT} and CASK^{4M} into human embryonic kidney (HEK) 293T cells, and the steady-state phosphorylation status of neurexin-1 was quantified (Fig. 5, C and D). As a control, we used tCASK, in which amino acids 1 to 161 have been deleted, severely truncating the kinase domain but leaving the MAGUK domains intact.

Surprisingly, neither autophosphorylation nor neurexin-1 phosphorylation at steady state was significantly augmented with $CASK^{4M}$ compared to $CASK^{WT}$ (Fig. 5, C and D). Thus, in the cytosol, CASK activity seems sufficient for maximum neurexin-1 phosphorylation. Most likely, the PDZ domain of CASK, which binds neurexin-1 (*10*), ensures a constant supply of substrate (*21*).

Based on the above observations, we suggest that the MAGUK scaffolding domains of CASK spatially constrain the CASK kinase activity to the vicinity of the membrane-bound cell adhesion protein complexes to which CASK binds. This scaffolding interaction not only raises the local substrate concentration and specificity, but also sustains stoichiometry between CASK and its substrate.

Evolution of CASK from a Mg^{2+}-coordinating kinase

The inability of Mg^{2+}-coordinating $CASK^{4M}$ to increase neurexin-1 phosphorylation in a cellular environment raises the possibility that the original CaMK domain, which merged with a MAGUK to give rise to an ancestral CASK kinase, could have been a canonical Mg^{2+}-coordinating enzyme. Thus, we searched for CASK-like sequences in evolutionarily ancient metazoan and animal species (fig. S7).

We detected the most ancient CASK proteins in basal metazoans, which typify the emergence of animals in evolution. A CASK ortholog was detected in the placozoan *Trichoplax adhaerens* (Fig. 6B), which lacks tissue differentiation but contains multiple neuronal proteins (*42*). Placozoan CASK shows canonical residues at three of the four positions we investigated as a source of Mg^{2+}-dependent inhibition in vertebrate CASK; at the 145-equivalent position in the catalytic loop, where vertebrate CASK carries a histidine instead of a glutamate, placozoan CASK features a glutamine. A similar Glu-to-Gln exchange is found in some active human CaMKs, such as DRAK-1 (DAP kinase–related apoptosis-inducing protein kinase 1) or -2, and is therefore compatible with a canonical Mg^{2+}-dependent kinase mechanism. Thus, placozoan CASK resembles $CASK^{4M}$ and may represent a Mg^{2+}-stimulated evolutionary CASK relic.

Cnidarians like *Nematostella vectensis*, the sea anemone, contain differentiated tissues, including neuronal tissue. The CASK ortholog of the sea anemone shows a single Glu-to-His substitution in the catalytic loop (Fig. 6A). Our CASK triple mutant (G162D-C146N-P22A), which is not stimulated by Mg^{2+} (Fig. 1), is most similar to the Cnidarian CASK.

All four of the amino acid changes we investigated first appear together in the subkingdom bilateria, as seen in platyhelminthes (*Schistosoma japonicum*), and are conserved thereafter. Curiously, ecdysozoans (molting animals), such as nematodes (*Caenorhabditis elegans*) and arthropods (*Drosophila melanogaster*), show sporadic variations in these substitutions (Fig. 6A), with functional implications that remain unclear.

Together, our phylogenetic analysis indicates that CASK arose from the fusion of a Mg^{2+}-coordinating CaMK domain with a membrane palmitoylated protein (MPP)–like scaffolding MAGUK. This fusion happened concurrently with the development of the basal metazoans. The substrate-scaffolding function provided by the MAGUK domains could then have allowed CASK to gradually shed its dependence on Mg^{2+}. These changes rendered CASK dependent on substrate recruitment through its MAGUK domains, such as the PDZ domain–dependent binding of neurexins.

DISCUSSION

Mammals contain at least 22 MAGUK proteins that vary in size and domain structure (*43*). MAGUKs are absent from bacterial, plant, fungal, and protozoan genomes, suggesting that their evolution coincided with the emergence of animals. CASK, the only MAGUK bearing a CaMK domain at its N-terminus, first appeared evolutionarily either simultaneous to, or shortly after, the emergence of MAGUKs in basal metazoans. Mutations in CASK are associated with numerous human developmental anomalies (*16*–*20*, *44*) and the *CASK* gene is essential in mice (*15*). Although CASK was considered a pseudokinase because of its lack of Mg^{2+} binding (*1*, *8*), we found that CASK is an active kinase and represents the first known kinase inhibited by Mg^{2+}, a cofactor of conventional kinases (*21*). In the present study, we examined the structural mechanism that confers on CASK its sensitivity to inhibition by Mg^{2+}. We identified four evolutionarily conserved residues that determine this property and showed that mutation of these residues converts Mg^{2+}'s inhibition of CASK into stimulation.

Pseudokinases constitute 10% of the human kinome. Many pseudokinases perform critical cellular functions, although before the identification of kinase activity in CASK, no pseudokinase was shown to be catalytically active. Moreover, previous attempts to convert pseudokinases into standard kinases through back mutation failed, possibly because of incomplete understanding of the precise evolutionary changes involved (*45*, *46*). Indeed, there are other pseudokinases (such as the Trb family of Ser-Thr kinases, and CCK4 tyrosine kinase) with substitutions in the Mg^{2+}-binding motifs analogous to those observed in CASK (*8*), and it is possible that these other pseudokinases may also be catalytically active under defined conditions. The mutations described here for $CASK^{4M}$ may also convert these other enzymes into Mg^{2+}-dependent kinases. Thus, similar to CASK, these atypical kinase domains may have accumulated changes that enable their specialization for a particular physiological niche.

Mg^{2+} has been postulated to promote kinase catalysis through facilitation of nucleotide binding, γ-phosphate positioning, and stabilization of the transition state. Our ability to generate a Mg^{2+}-coordinating mutant of CASK, $CASK^{4M}$, in which Mg^{2+} strongly accelerated phosphate transfer, allowed us to directly address the mechanisms of Mg^{2+}-dependent catalytic enhancement. Analysis of crystal structures together with enzymatic studies suggested that Mg^{2+} acts primarily downstream of ATP binding by binding to its β-phosphate. Direct binding to the β-phosphate suggests roles of Mg^{2+} in stabilization of the transition state and compensation of the additional negative charge evolving at the β-phosphate during phosphate transfer (thus enhancing the property of ADP as a leaving group) during catalysis. Mg^{2+} may also indirectly alter the positioning of the γ-phosphate of bound ATP.

Phylogenetically, the CASK CaMK domain falls near the CaMKII cluster (*1*), members of which are autoinhibited by a Ca^{2+}-CaM–dependent regulatory domain (*27*). However, unlike CaMKII, an Arg-to-Leu substitution present in even the most primitive placozoan CASK renders its autoregulatory segment suboptimal for competing with substrate binding. Moreover, unlike CaMKII (*27*), CASK exhibits no dimerization of the autoregulatory domain and constitutively adopts an active, closed conformation. This conformation permits uninterrupted ATP binding to the CASK nucleotide-binding pocket, possibly compensating in part for the suboptimal, Mg^{2+}-independent phosphotransfer chemistry used by the enzyme.

Moreover, the merger of an ancestral CASK kinase domain with a MAGUK linked the enzyme activity to the MAGUK scaffolding domains, which could recruit substrate, thereby (i) facilitating phosphotransfer by increasing the local substrate concentration, (ii) increasing substrate specificity (*9*), and (iii) eliminating the need for fast catalytic turnover (Fig. 6C). Based on the above features, the CASK catalytic site has continuous access to both ATP and its protein substrate, rendering the enzyme independent of both Mg^{2+} and Ca^{2+}.

The presence of Mg^{2+}-coordinating residues in placozoan CASK suggests that the lack of stimulation of CASK by Mg^{2+} was acquired after, and possibly as a result of, its independence from divalent ions. The primary change contributing to lack of stimulation by Mg^{2+}seems to be the acquisition of a His^{145} equivalent in the nucleotide-binding pocket,

A

CaMKII-α	T. adhaerens	N. vectensis	C. elegans	D. melanogaster	S. japonicum	L. stagnalis	S. kowalevskii	D. rerio	X. laevis	G. gallus	M. musculus	H. sapiens	CASK-4M	Residue
Ala	Ala	Thr	Pro	Pro	Pro	Pro	Pro	Pro	Pro	Pro	Pro	Pro	Ala	22
Glu	Gln	His	His	Ala	His	His	His	His	His	His	His	His	Glu	145
Asn	Asn	Asn	Asn	Cys	Cys	Cys	Cys	Cys	Cys	Cys	Cys	Cys	Asn	146
Asp	Asp	Asp	Gly	Gly	Gly	Gly	Gly	Gly	Gly	Gly	Gly	Gly	Asp	162

B

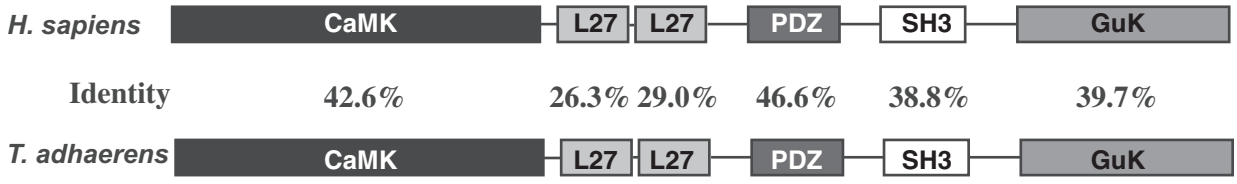

C

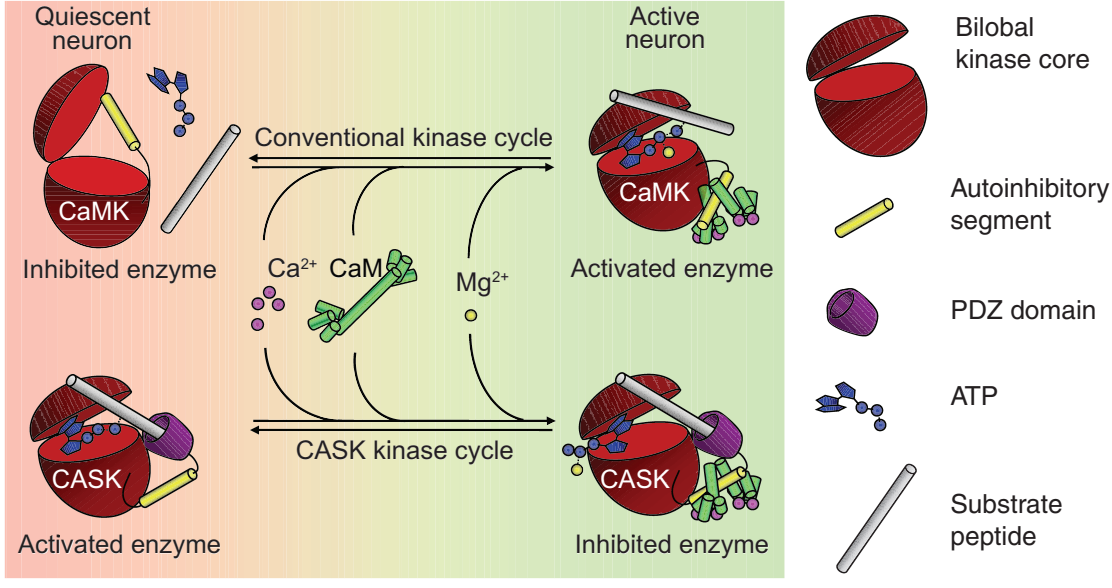

Fig. 6. CASK evolution. (A) Evolutionary changes in the nucleotide-binding pocket of CASK CaMK domain. CASK CaMK domain sequences from various animal species were aligned, and the residues corresponding to those mutated in CASK^{4M} were identified and are shown. Corresponding human CaMKII-α residues are shown on the left for comparison. (B) Sequence conservation (identities) of CASK domains between human and placozoan CASK (from *T. adhaerens*). See fig. S7 for a full sequence alignment. (C) Model comparing CASK and CaMKI catalytic cycles. Typically, CaMKs are held in an autoinhibited conformation by the autoregulatory domain (yellow) with an open, inactive nucleotide-binding cleft. Upon binding of Ca^{2+} (purple)–CaM (green), this autoinhibition is relieved and the enzyme attains an active closed conformation amenable to Mg^{2+} (yellow)–ATP (blue) binding and substrate binding. CASK CaMK domain, by contrast, constitutively binds ATP, and is regulated by the recruitment of its substrates through the MAGUK scaffolding domains, especially the PDZ domain.

which appears to be critical to counteract Mg^{2+} coordination. This change may have caused a lack of evolutionary pressure to maintain a flexible glycine-rich (GR) loop or Mg^{2+}-coordinating residues elsewhere in the domain, thus inviting secondary changes in the nucleotide-binding pocket. Once optimized over the evolutionary time scale, this domain architecture was maintained in all chordates.

Why was CASK transformed from a putative Mg^{2+}-stimulated to a Mg^{2+}-inhibited kinase early in evolution? One possibility is that Mg^{2+}

was unnecessary in the context of the substrate-recruiting mechanism implemented by the MAGUK domains of CASK (*21*). Consistent with this idea, our experiments in cells (Fig. 5C) demonstrate that Mg^{2+} stimulation does not confer increased steady-state phosphorylation in a cellular context in which the substrate is recruited by the PDZ domain. An additional possibility is that inhibition by divalent ions evolved with the emergence of excitable cells, such as those in the nervous system, as a mechanism of negative regulation. Localized influx of divalent ions might reduce the free ATP concentration at a synapse, thereby slowing CASK's catalytic rate (Fig. 6C). Together, it appears that the multidomain structure of CASK allowed the CaMK domain to shed its Mg^{2+} dependence, which led to evolution of CASK into a hybrid kinase, with a substrate-recruitment module (the PDZ domain) fused to a slow, regulated catalytic module (the CaMK domain).

MATERIALS AND METHODS

Mutagenesis and recombinant protein production

pGEX-CASK$^{1–337}$ and its point mutations generated with the QuikChange site-directed mutagenesis kit (Stratagene) were used to express the protein glutathione *S*-transferase (GST)–CASK$^{1–337}$ (GST-CASK CaMK domain) and the corresponding mutant proteins in *Escherichia coli* strain BL21. The expression products were affinity-purified with glutathione Sepharose beads (Amersham Biosciences). CASK CaMK domain and its mutants were cleaved from the beads with thrombin. The proteins were further purified through a Superdex 200 size-exclusion column on an ÄKTA FPLC station (Amersham Biosciences) with 10 mM Hepes-KOH (pH 7.4), 1 mM dithiothreitol (DTT), 10% glycerol, and 100 mM KCl as the running buffer and concentrated to 15 mg/ml by ultrafiltration (Amicon). Such protein preparations, which absorbed strongly at 260 nm, were used for crystallographic studies. For nucleotide binding experiments the proteins were further precipitated by 25% saturated ammonium sulfate solution to remove bound nucleic acids and nucleotides. The precipitated proteins were resuspended in 10 mM tris-HCl (pH 7.2), 10% glycerol, 1 mM DTT, and 100 mM KCl. CaMKII was a gift from R. J. Colbran (Vanderbilt University).

KinaseGlo assay

Indicated proteins (1 μM), autocamtide-2 (100 μM), and ATP were incubated for 60 min in tris-HCl buffer (pH 6.8) supplemented with Mg^{2+} (2 mM), Ca^{2+} (1 mM), and CaM (4 μM),. The amount of ATP remaining was detected with a stabilized luciferase-luciferin–based reagent (KinaseGlo, Promega) according to the manufacturer's protocol. Luminescence was detected with an Orion microplate reader (Berthold Detection Systems).

TNP-ATP-CASK CaMK domain binding assay

TNP-ATP, which becomes fluorescent when inserted into the hydrophobic ATP-binding pocket of protein kinases (*47*), was acquired from Molecular Probes Inc. Experiments were performed in 50 mM tris-HCl (pH 7.2) and 50 mM KCl in 1 cm × 1 cm fluorescence cuvettes at 25°C with a Jobin Yvon-Spex Fluoromax-2 (*47*). Samples were excited at 410 nm and emission spectra were scanned from 500 to 600 nm. Excitation and emission slits were set at 3 and 5 nm, respectively. For TNP-ATP titration experiments, fluorescence emission at 541 nm was measured and corrected by subtracting the signal from a TNP-ATP buffer control, in which lysozyme replaced CASK CaMK domain.

In vitro autophosphorylation assays

Recombinant CASK CaMK domain (1 μM) was incubated for 2 hours in the tris-HCl buffer supplemented with 10 mM Mg^{2+}-[γ-^{32}P]ATP or 10 mM Na^{+}- [γ-^{32}P]ATP (50 cpm/pmol) in a reaction volume of 25 μl at 30°C with shaking. The proteins were separated by SDS–polyacrylamide gel electrophoresis (SDS-PAGE), transferred to a nitrocellulose membrane, and visualized with a phosphorimager (Molecular Dynamics Storm scanner and Image-Quant software). Mock experiments were used to determine protein estimation by Coomassie.

We followed a modification of the protocol of Fujimoto *et al.* (*48*), in which we used glutaraldehyde-treated nitrocellulose membrane (*49*), to assess phosphate transfer onto substrate peptide. Briefly, protein was incubated with [γ-^{32}P]ATP, $MgCl_2$, and 100 μM autocamtide-2. The reaction was stopped with 1% SDS and the mixture was blotted onto a nitrocellulose membrane. The peptide was fixed to a nitrocellulose membrane with 0.2% glutaraldehyde. The membranes were extensively washed in tris-buffered saline–Tween 20 and counts were obtained on a scintillation counter (Beckman Coulter LS 6500). Michaelis constant (K_m^{ATP}) and V_{max} were calculated with GraphPad Prism software. Statistical significance was evaluated with Student's *t* test.

Crystallization and data collection

The CASK^{4M} CaMK domain was crystallized like the wild type CASK CaMK domain by the sitting-drop vapor-diffusion method at room temperature (*21*). Drops composed of 1 μl of protein solution and 1μl of reservoir were equilibrated against 0.5 ml of a reservoir consisting of 12.5% (v/v) ethylene glycol. Crystals appeared after several days. All crystals used in this study belonged to space group $P2_12_12_1$ and could be frozen in a liquid nitrogen stream after increasing the ethylene glycol content of the mother liquor to 25% (v/v). For Mn^{2+} and nucleotide binding analyses, crystals were incubated for 15 min in 25% (v/v) ethylene glycol supplemented with 10 mM $MnCl_2$ or 10 mM AMPPNP, or with both, and then immediately flash-frozen. Diffraction data were recorded on beam line BL14.2 of BESSY with a mar225 charged-coupled device detector (MarResearch). Data were processed with the HKL package (*50*) (Table 1).

Structure solution and refinement

The structures of all forms of the CASK^{4M} CaMK domain were solved by molecular replacement with the program MolRep (*51*). The structure of wild-type CASK CaMK domain [PDB ID 3C0I (*21*)] without nucleotide and water molecules was used as the search model. Automated refinement was conducted with Refmac5 (*52*), alternating with manual model building using Coot (*53*). The placed models were first adjusted as rigid bodies and subsequently refined by positional and temperature factor refinement. The models were manually rebuilt with $2F_o - F_c$ and $F_o - F_c$ electron density maps, including manual exchange of the mutated residues. In the co-crystal structures, nucleotide or Mn^{2+} or both were positioned into clear patches of electron density in the nucleotide binding clefts. Water molecules were automatically placed with ARP/wARP software (*54*) (EMBL). We verified by manual inspection that water molecules occupied spherical peaks of the electron density in hydrogen-bonding distance to protein atoms. In the final rounds of refinement, we included TLS refinement (*55*), in which the models were dissected into two TLS groups (corresponding to the N-terminal and C-terminal lobes), for which independent anisotropic temperature factor corrections were applied. The above structure solution, model building, and refinement procedure progressed smoothly for all structures and yielded low R/R_{free} factors, while at the same time conserving good stereochemistry in the models (Table 1).

In vivo kinase activity assays

The complementary DNAs (cDNAs) encoding CASK^{WT} and CASK^{4M} were inserted into plasmid pEGFP-C3 to generate the fusion proteins

EGFP-CASK^{WT} and EGFP-CASK^{4M}. To generate EGFP-tCASK, the first half of the CaMK kinase domain (residues 1 to 161) was removed from pEGFP-CASK^{WT} using the Hind III site.

HEK293T cells were cotransfected with pEGFP-CASK and neurexin-1β-flag in pCMV vector with FUGENE-6 (Roche). Two days after transfection, the cells were washed and incubated in phosphate-free depletion buffer for 30 min at 37°C [10 mM Hepes-NaOH (pH 7.2), 150 mM NaCl, 4 mM KCl, 2 mM $MgCl_2$, and 2 mM $CaCl_2$], followed by incubation in the same buffer supplemented with 100 μCi [^{32}P]orthophosphate for 1 hour. Cells were washed twice with phosphate-free buffer and lysed in ice-cold solubilization buffer [10 mM tris-HCl (pH 6.8), 150 mM NaCl, 1% Triton X-100, and 4 mM EDTA] supplemented with protease inhibitor cocktail (leupeptin, pepstatin, phenylmethylsulfonyl fluoride, and aprotinin) and phosphatase inhibitor cocktails 1 and 2 (Sigma). Debris was spun down (14,000 rpm for 10 min at 4°C) and the supernatant was incubated with M2 beads (Sigma). Complexes were washed three times in solubilization buffer and separated by SDS-PAGE, followed by phosphorimager scanning. β-Neurexin and CASK immunoblots were used to control loading.

SUPPLEMENTARY MATERIALS

www.sciencesignaling.org/cgi/content/full/3/119/ra33/DC1
Fig. S1. Specificity of TNP-ATP binding.
Fig. S2. Autophosphorylation of wild-type (WT) and mutant CASK CaMK domains.
Fig. S3. TNP-ATP binding.
Fig. S4. Autophosphorylation of the CASK^{4M} CaMK domain in the presence of Mg^{2+}.
Fig. S5. Stereo plots showing close-ups of the nucleotide-binding pocket of CASK^{4M} CaMK.
Fig. S6. Regulatory segment of the CASK CaMK domain.
Fig. S7. Sequence alignment of CASK orthologs.

REFERENCES AND NOTES

1. G. Manning, D. B. Whyte, R. Martinez, T. Hunter, S. Sudarsanam, The protein kinase complement of the human genome. *Science* **298**, 1912–1934 (2002).
2. M. E. Noble, J. A. Endicott, L. N. Johnson, Protein kinase inhibitors: Insights into drug design from structure. *Science* **303**, 1800–1805 (2004).
3. M. Huse, J. Kuriyan, The conformational plasticity of protein kinases. *Cell* **109**, 275–282 (2002).
4. S. K. Hanks, A. M. Quinn, T. Hunter, The protein kinase family: Conserved features and deduced phylogeny of the catalytic domains. *Science* **241**, 42–52 (1988).
5. S. S. Taylor, E. Radzio-Andzelm, Three protein kinase structures define a common motif. *Structure* **2**, 345–355 (1994).
6. J. M. Higgins, Haspin-like proteins: A new family of evolutionarily conserved putative eukaryotic protein kinases. *Protein Sci.* **10**, 1677–1684 (2001).
7. O. Mayans, P. F. van der Ven, M. Wilm, A. Mues, P. Young, D. O. Furst, M. Wilmanns, M. Gautel, Structural basis for activation of the titin kinase domain during myofibrillogenesis. *Nature* **395**, 863–869 (1998).
8. J. Boudeau, D. Miranda-Saavedra, G. J. Barton, D. R. Alessi, Emerging roles of pseudokinases. *Trends Cell Biol.* **16**, 443–452 (2006).
9. J. A. Ubersax, J. E. Ferrell Jr., Mechanisms of specificity in protein phosphorylation. *Nat. Rev. Mol. Cell Biol.* **8**, 530–541 (2007).
10. Y. Hata, S. Butz, T. C. Südhof, CASK: A novel dlg/PSD95 homolog with an N-terminal calmodulin-dependent protein kinase domain identified by interaction with neurexins. *J. Neurosci.* **16**, 2488–2494 (1996).
11. A. R. Cohen, D. F. Woods, S. M. Marfatia, Z. Walther, A. H. Chishti, J. M. Anderson, Human CASK/LIN-2 binds syndecan-2 and protein 4.1 and localizes to the basolateral membrane of epithelial cells. *J. Cell Biol.* **142**, 129–138 (1998).
12. Y. P. Hsueh, T. F. Wang, F. C. Yang, M. Sheng, Nuclear translocation and transcription regulation by the membrane-associated guanylate kinase CASK/LIN-2. *Nature* **404**, 298–302 (2000).
13. Y. P. Hsueh, F. C. Yang, V. Kharazia, S. Naisbitt, A. R. Cohen, R. J. Weinberg, M. Sheng, Direct interaction of CASK/LIN-2 and syndecan heparan sulfate proteoglycan and their overlapping distribution in neuronal synapses. *J. Cell Biol.* **142**, 139–151 (1998).
14. T. Biederer, Y. Sara, M. Mozhayeva, D. Atasoy, X. Liu, E. T. Kavalali, T. C. Südhof, SynCAM, a synaptic adhesion molecule that drives synapse assembly. *Science* **297**, 1525–1531 (2002).
15. D. Atasoy, S. Schoch, A. Ho, K. A. Nadasy, X. Liu, W. Zhang, K. Mukherjee, E. D. Nosyreva, R. Fernandez-Chacon, M. Missler, E. T. Kavalali, T. C. Südhof, Deletion of CASK in mice is lethal and impairs synaptic function. *Proc. Natl. Acad. Sci. U.S.A.* **104**, 2525–2530 (2007).
16. S. D. Dimitratos, D. G. Stathakis, C. A. Nelson, D. F. Woods, P. J. Bryant, The location of human *CASK* at Xp11.4 identifies this gene as a candidate for X-linked optic atrophy. *Genomics* **51**, 308–309 (1998).
17. G. Froyen, H. Van Esch, M. Bauters, K. Hollanders, S. G. Frints, J. R. Vermeesch, K. Devriendt, J. P. Fryns, P. Marynen, Detection of genomic copy number changes in patients with idiopathic mental retardation by high-resolution X-array-CGH: Important role for increased gene dosage of *XLMR* genes. *Hum. Mutat.* **28**, 1034–1042 (2007).
18. S. Hayashi, S. Mizuno, O. Migita, T. Okuyama, Y. Makita, A. Hata, I. Imoto, J. Inazawa, The CASK gene harbored in a deletion detected by array-CGH as a potential candidate for a gene causative of X-linked dominant mental retardation. *Am. J. Med. Genet. A* **146A**, 2145–2151 (2008).
19. J. Najm, D. Horn, I. Wimplinger, J. A. Golden, V. V. Chizhikov, J. Sudi, S. L. Christian, R. Ullmann, A. Kuechler, C. A. Haas, A. Flubacher, L. R. Charnas, G. Uyanik, U. Frank, E. Klopocki, W. B. Dobyns, K. Kutsche, Mutations of CASK cause an X-linked brain malformation phenotype with microcephaly and hypoplasia of the brainstem and cerebellum. *Nat. Genet.* **40**, 1065–1067 (2008).
20. B. A. Samuels, Y. P. Hsueh, T. Shu, H. Liang, H. C. Tseng, C. J. Hong, S. C. Su, J. Volker, R. L. Neve, D. T. Yue, L. H. Tsai, Cdk5 promotes synaptogenesis by regulating the subcellular distribution of the MAGUK family member CASK. *Neuron* **56**, 823–837 (2007).
21. K. Mukherjee, M. Sharma, H. Urlaub, G. P. Bourenkov, R. Jahn, T. C. Südhof, M. C. Wahl, CASK functions as a Mg^{2+}-independent neurexin kinase. *Cell* **133**, 328–339 (2008).
22. J. A. Adams, Kinetic and catalytic mechanisms of protein kinases. *Chem. Rev.* **101**, 2271–2290 (2001).
23. S. K. Hanks, T. Hunter, Protein kinases 6. The eukaryotic protein kinase superfamily: Kinase (catalytic) domain structure and classification. *FASEB J.* **9**, 576–596 (1995).
24. J. A. Adams, S. S. Taylor, Divalent metal ions influence catalysis and active-site accessibility in the cAMP-dependent protein kinase. *Protein Sci.* **2**, 2177–2186 (1993).
25. Y. Cheng, Y. Zhang, J. A. McCammon, How does the cAMP-dependent protein kinase catalyze the phosphorylation reaction: An ab initio QM/MM study. *J. Am. Chem. Soc.* **127**, 1553–1562 (2005).
26. P. Saylor, C. Wang, T. J. Hirai, J. A. Adams, A second magnesium ion is critical for ATP binding in the kinase domain of the oncoprotein v-Fps. *Biochemistry* **37**, 12624–12630 (1998).
27. O. S. Rosenberg, S. Deindl, R. J. Sung, A. C. Nairn, J. Kuriyan, Structure of the autoinhibited kinase domain of CaMKII and SAXS analysis of the holoenzyme. *Cell* **123**, 849–860 (2005).
28. F. W. Herberg, M. L. Doyle, S. Cox, S. S. Taylor, Dissection of the nucleotide and metal-phosphate binding sites in cAMP-dependent protein kinase. *Biochemistry* **38**, 6352–6360 (1999).
29. N. Narayana, S. Cox, X. Nguyen-huu, L. F. Ten Eyck, S. S. Taylor, A binary complex of the catalytic subunit of cAMP-dependent protein kinase and adenosine further defines conformational flexibility. *Structure* **5**, 921–935 (1997).
30. W. F. Waas, M. A. Rainey, A. E. Szafranska, K. Cox, K. N. Dalby, A kinetic approach towards understanding substrate interactions and the catalytic mechanism of the serine/threonine protein kinase ERK2: Identifying a potential regulatory role for divalent magnesium. *Biochim. Biophys. Acta* **1697**, 81–87 (2004).
31. J. F. Ohren, H. Chen, A. Pavlovsky, C. Whitehead, E. Zhang, P. Kuffa, C. Yan, P. McConnell, C. Spessard, C. Banotai, W. T. Mueller, A. Delaney, C. Omer, J. Sebolt-Leopold, D. T. Dudley, I. K. Leung, C. Flamme, J. Warmus, M. Kaufman, S. Barrett, H. Tecle, C. A. Hasemann, Structures of human MAP kinase kinase 1 (MEK1) and MEK2 describe novel noncompetitive kinase inhibition. *Nat. Struct. Mol. Biol.* **11**, 1192–1197 (2004).
32. V. Tereshko, M. Teplova, J. Brunzelle, D. M. Watterson, M. Egli, Crystal structures of the catalytic domain of human protein kinase associated with apoptosis and tumor suppression. *Nat. Struct. Biol.* **8**, 899–907 (2001).
33. K. Niefind, B. Guerra, I. Ermakowa, O. G. Issinger, Crystal structure of human protein kinase CK2: Insights into basic properties of the CK2 holoenzyme. *EMBO J.* **20**, 5320–5331 (2001).
34. M. Valiev, J. Yang, J. A. Adams, S. S. Taylor, J. H. Weare, Phosphorylation reaction in cAPK protein kinase-free energy quantum mechanical/molecular mechanics simulations. *J. Phys. Chem. B* **111**, 13455–13464 (2007).
35. R. Battistutta, E. De Moliner, S. Sarno, G. Zanotti, L. A. Pinna, Structural features underlying selective inhibition of protein kinase CK2 by ATP site-directed tetrabromo-2-benzotriazole. *Protein Sci.* **10**, 2200–2206 (2001).
36. K. C. Qian, L. Wang, E. R. Hickey, J. Studts, K. Barringer, C. Peng, A. Kronkaitis, J. Li, A. White, S. Mische, B. Farmer, Structural basis of constitutive activity and a unique nucleotide binding mode of human Pim-1 kinase. *J. Biol. Chem.* **280**, 6130–6137 (2005).
37. B. Nolen, S. Taylor, G. Ghosh, Regulation of protein kinases; controlling activity through activation segment conformation. *Mol. Cell* **15**, 661–675 (2004).
38. J. Goldberg, A. C. Nairn, J. Kuriyan, Structural basis for the autoinhibition of calcium/calmodulin-dependent protein kinase I. *Cell* **84**, 875–887 (1996).

39. Y. L. Fong, T. R. Soderling, Studies on the regulatory domain of Ca^{2+}/calmodulin-dependent protein kinase II. Functional analyses of arginine 283 using synthetic inhibitory peptides and site-directed mutagenesis of the α subunit. *J. Biol. Chem.* **265**, 11091–11097 (1990).
40. M. K. Smith, R. J. Colbran, D. A. Brickey, T. R. Soderling, Functional determinants in the autoinhibitory domain of calcium/calmodulin-dependent protein kinase II. Role of His^{282} and multiple basic residues. *J. Biol. Chem.* **267**, 1761–1768 (1992).
41. O. Miyano, I. Kameshita, H. Fujisawa, Purification and characterization of a brain-specific multifunctional calmodulin-dependent protein kinase from rat cerebellum. *J. Biol. Chem.* **267**, 1198–1203 (1992).
42. M. Srivastava, E. Begovic, J. Chapman, N. H. Putnam, U. Hellsten, T. Kawashima, A. Kuo, T. Mitros, A. Salamov, M. L. Carpenter, A. Y. Signorovitch, M. A. Moreno, K. Kamm, J. Grimwood, J. Schmutz, H. Shapiro, I. V. Grigoriev, L. W. Buss, B. Schierwater, S. L. Dellaporta, D. S. Rokhsar, The *Trichoplax* genome and the nature of placozoans. *Nature* **454**, 955–960 (2008).
43. A. J. te Velthuis, J. F. Admiraal, C. P. Bagowski, Molecular evolution of the MAGUK family in metazoan genomes. *BMC Evol. Biol.* **7**, 129 (2007).
44. Q. Wang, J. Lu, C. Yang, X. Wang, L. Cheng, G. Hu, Y. Sun, X. Zhang, M. Wu, Z. Liu, CASK and its target gene Reelin were co-upregulated in human esophageal carcinoma. *Cancer Lett.* **179**, 71–77 (2002).
45. J. Boudeau, J. W. Scott, N. Resta, M. Deak, A. Kieloch, D. Komander, D. G. Hardie, A. R. Prescott, D. M. van Aalten, D. R. Alessi, Analysis of the LKB1-STRAD-MO25 complex. *J. Cell Sci.* **117**, 6365–6375 (2004).
46. S. A. Prigent, W. J. Gullick, Identification of c-erbB-3 binding sites for phosphatidylinositol 3′-kinase and SHC using an EGF receptor/c-erbB-3 chimera. *EMBO J.* **13**, 2831–2841 (1994).
47. R. C. Stewart, R. VanBruggen, D. D. Ellefson, A. J. Wolfe, TNP-ATP and TNP-ADP as probes of the nucleotide binding site of CheA, the histidine protein kinase in the chemotaxis signal transduction pathway of *Escherichia coli*. *Biochemistry* **37**, 12269–12279 (1998).
48. M. Fujimoto, Y. Kuwano, R. Watanabe, N. Asashima, H. Nakashima, S. Yoshitake, H. Okochi, K. Tamaki, J. C. Poe, T. F. Tedder, S. Sato, B cell antigen receptor and CD40 differentially regulate CD22 tyrosine phosphorylation. *J. Immunol.* **176**, 873–879 (2006).
49. Z. Wang, G. Dong, S. Singh, H. Steen, J. Li, A simple and effective method for detecting phosphopeptides for phosphoproteomic analysis. *J. Proteomics* **72**, 831–835 (2009).
50. Z. Otwinowski, W. Minor, Processing of X-ray diffraction data collected in oscillation mode. *Methods Enzymol.* **276**, 307–326 (1997).
51. A. Vagin, A. Teplyakov, An approach to multi-copy search in molecular replacement. *Acta Crystallogr. D Biol. Crystallogr.* **56**, 1622–1624 (2000).
52. G. N. Murshudov, A. A. Vagin, E. J. Dodson, Refinement of macromolecular structures by the maximum-likelihood method. *Acta Crystallogr. D Biol. Crystallogr.* **53**, 240–255 (1997).
53. P. Emsley, K. Cowtan, Coot: Model-building tools for molecular graphics. *Acta Crystallogr. D Biol. Crystallogr.* **60**, 2126–2132 (2004).
54. G. Langer, S. X. Cohen, V. S. Lamzin, A. Perrakis, Automated macromolecular model building for X-ray crystallography using ARP/wARP version 7. *Nat. Protoc.* **3**, 1171–1179 (2008).
55. M. D. Winn, M. N. Isupov, G. N. Murshudov, Use of TLS parameters to model anisotropic displacements in macromolecular refinement. *Acta Crystallogr. D Biol. Crystallogr.* **57**, 122–133 (2001).

56. **Acknowledgments:** We thank members of the Südhof and Jahn laboratories for discussions and R. Lührmann for providing access to crystallography equipment. We are grateful to the support by the staff of beam line BL14.2 (BESSY) for help during collection of diffraction data. **Funding:** This work was supported by a grant from the National Institute of Mental Health (R37 MH52804-08 to T.C.S.) and the Max-Planck-Society. M.S. is a Human Frontier Long Term Fellow. **Author contributions:** K.M., M.S., and M.C.W. designed and performed the experiments, analyzed data, and wrote the manuscript. R.J. designed the experiments. T.C.S. designed the experiments, analyzed data, and wrote the manuscript. **Accession numbers:** Atomic coordinates have been deposited with the PDB; accession numbers are 3MFR, 3MFS, 3MFT, and 3MFU.

Submitted 22 December 2009
Accepted 9 April 2010
Final Publication 27 April 2010
10.1126/scisignal.2000800
Citation: K. Mukherjee, M. Sharma, R. Jahn, M. C. Wahl, T. C. Südhof, Evolution of CASK into a Mg^{2+}-sensitive kinase. *Sci. Signal.* **3**, ra33 (2010).